

Sustainable Food Technology

Accepted Manuscript

This article can be cited before page numbers have been issued, to do this please use: R. Mishra, S. Jangra, A. Mishra, S. Pandey, M. Chhabra and R. Prakash, *Sustainable Food Technol.*, 2025, DOI: 10.1039/D5FB00584A.



This is an Accepted Manuscript, which has been through the Royal Society of Chemistry peer review process and has been accepted for publication.

Accepted Manuscripts are published online shortly after acceptance, before technical editing, formatting and proof reading. Using this free service, authors can make their results available to the community, in citable form, before we publish the edited article. We will replace this Accepted Manuscript with the edited and formatted Advance Article as soon as it is available.

You can find more information about Accepted Manuscripts in the [Information for Authors](#).

Please note that technical editing may introduce minor changes to the text and/or graphics, which may alter content. The journal's standard [Terms & Conditions](#) and the [Ethical guidelines](#) still apply. In no event shall the Royal Society of Chemistry be held responsible for any errors or omissions in this Accepted Manuscript or any consequences arising from the use of any information it contains.

Sustainability Spotlight Statement

Millets are climate-resilient, nutrient-dense grains critical for global food and nutrition security, yet their wider use is limited by processing challenges. Conventional processing often depletes nutrients and demands high energy, contradicting sustainable practices. This study demonstrates the application of non-equilibrium cold plasma (NECP), a non-thermal, chemical-free, and energy-efficient technology, to enhance the functional and thermal properties of pearl and sorghum millet flours without compromising quality. By improving flour performance for gluten-free and functional food applications, the work promotes sustainable food diversification and supports resilient food systems. This aligns with UN Sustainable Development Goals (SDG 2: Zero Hunger, SDG 3: Good Health and Well-being, and SDG 12: Responsible Consumption and Production).

View Article Online

DOI: 10.1039/D5FB00584A

Non-Equilibrium Cold Plasma as a Sustainable Approach to Improve Functional and Thermal Properties of Pearl and Sorghum Millet Flours

Ritesh Mishra¹, Sushma Jangra², Abhijit Mishra², Shikha Pandey², Meenu Chhabra^{3,1}, and Ram Prakash^{2,1}

¹Inter-Disciplinary Research Division-Smart Healthcare, Indian Institute of Technology, Jodhpur, Rajasthan, India

²Department of Physics, Indian Institute of Technology, Jodhpur, Rajasthan, India

³Department of Bioscience and Bioengineering, Indian Institute of Technology, Jodhpur, Rajasthan, India

*Corresponding Author e-mail: ramprakash@iitj.ac.in

Abstract

This study investigates the effects of non-equilibrium cold plasma (NECP) treatment using air plasma and transient exposure methods on the functional, structural, and thermal properties of pearl and sorghum millet flours. Pearl and sorghum millet flour were treated at two different exposure times for 5 min and 10 min, and functional properties such as Water and oil holding capacity, water binding capacity, color, and dispersibility of the control and plasma-treated flour were studied. There was no significant difference in the color intensity and the whitening index (WI) with the treatment. However, the 10-minute treatment resulted in an increase in water absorption capacity (1.55–1.81 g/g), oil absorption capacity (1.21–1.4 g/g), and water binding capacity (2.25–2.37 g/g) in pearl millet flour. Similarly, sorghum millet flour water absorption capacity (1.43 to 1.74 g/g), oil absorption capacity (1.08 to 1.27 g/g), and water binding capacity (2.07–2.26 g/g) increase with 10 min NECP treatment. In addition, Fourier transform infrared spectrometry analysis detected shifts in functional groups, X-ray diffraction analysis indicated changes in crystallinity, and Differential crystallography showed a reduction in gelatinization enthalpy. Overall, plasma treatment can be explored for the development of a process to enhance the functionality of millet flour for applications in food systems.

Keywords: Non-equilibrium cold plasma, pearl millet flour, sorghum millet flour, functional properties, thermal properties

31 **1. Introduction**

32 Millets, a type of grass, are distinguished by their compact, slender stems and minuscule seeds,
33 both of which exhibit remarkable resistance to extended periods of drought. Millets are
34 considered to be among the earliest cereal grains farmed for the sake of subsistence (1). Millets
35 are widely known as "smart food." Millets are a highly nutritious food, rich in iron, folate,
36 calcium, zinc, magnesium, phosphorus, copper, vitamins, fiber, and antioxidants. In addition,
37 besides being essential for the proper development and maturation of children, they have been
38 shown to reduce the risk of heart disease and diabetes in adults. In addition, Millet is a suitable
39 choice for individuals with coeliac disease or gluten-related illnesses such as wheat allergy and
40 non-celiac gluten sensitivity, which can have significant health consequences when even little
41 amounts of gluten are consumed (2). There has been a rise in demand for gluten-free products
42 among individuals seeking to adhere to a nutritious diet. To achieve this, it is imperative to
43 enhance and broaden the food business by advancing the development of ingredients and
44 formulations, as well as increasing the production of functional foods (3). Sorghum (*Sorghum*
45 *bicolor*) and Pearl millet (*Pennisetum glaucum*) are two significant millet varieties that are
46 renowned for their nutritional advantages and are frequently utilized for producing gluten-free
47 flour. These grains are currently receiving more attention from food scientists, nutritionists,
48 and policymakers because of their socio-economic consequences (4). To globally promote and
49 popularize these millets, it is essential to create advanced processing techniques that
50 specifically aim to increase the functional and structural properties of millet flour. However,
51 the emphasis on the processing and enhancement of millet flours is currently limited due to the
52 lack of awareness regarding their nutritional and health advantages among the population.
53 While various research has employed boiling, microwave treatment, cooking, and autoclaving
54 for processing (5). These technologies adversely affect the nutritional properties of the flour.
55 This has urged the need to investigate the applicability of non-thermal technologies like cold
56 plasma.

57 Non-equilibrium Cold plasma (NECP) treatment is a highly adaptable method that can be used
58 in various applications in the food industry. It can be used to modify the structure of
59 macromolecules like starch, protein, and cellulose, promote seed germination, eliminate
60 microbes, and extract bioactive chemicals (6). The NECP treatment is an acknowledged non-
61 thermal technology, classified as the fourth state of matter. It is a partially ionized gas that
62 consists of free radicals, photons, ozone, energetic ions, and free electrons in either the ground



63 or excited state (7–9). The studies reported that the treatment of cold plasma had a significant
64 impact on the functional, rheological, and thermal properties of various types of flour,
65 including wheat flour, quinoa flour, jackfruit seed flour, little millet flour, and bamboo rice
66 flour (10–15). However, there has been little research conducted on the effects of various
67 treatment conditions on the nutritional and antinutritional components, as well as the functional
68 and thermal properties of millet flours. R et al. (2021) (16) exposed the pearl millet to cold
69 plasma technology at 180 V with a 0.01 m³/h airflow rate. The study concluded that the phytic
70 acid content was reduced by 60.66% and 39.27% when the treatment was operated on for 1
71 and 2 h, respectively. Jaddu, Pradhan et al. (2022) (12) reported that the crystallinity of the
72 little millet flour reduces due to the depolymerization of starch during the cold plasma
73 treatment. They also showed that the treatment increased the water absorption capacity (WAC),
74 oil absorption capacity (OAC), swelling capacity, and solubility index of the flour. The impacts
75 of ultra-high pressure coupled with cold plasma treatment on physical, chemical, and digestive
76 qualities are investigated in another research on proso millet starch (17).

77 Previous studies on flour properties utilized either a pin-type or a multipin cold plasma setup
78 (18–23). This device has the capability to generate plasma distributions that are not uniform,
79 resulting in uneven treatment over the surface area. The treatment region for pin-type devices
80 is often confined to the immediate vicinity of the pin electrodes. When dealing with big regions
81 or volumes, it is necessary to either make many passes or use an array of pins, which makes
82 the operation more complex. Attaining a fully homogeneous plasma treatment might be
83 challenging, even with the utilization of several pins. Inconsistent treatment effects can result
84 from variations in plasma intensity among pins. Moreover, the intense concentration of energy
85 around the pin electrodes can lead to localized surface harm or deterioration, particularly for
86 delicate materials. In addition, Pin electrodes are prone to experiencing wear and erosion as
87 time passes, which requires frequent maintenance and replacement. This leads to higher
88 operational expenses and periods of inactivity. In contrast to earlier investigations, air plasma
89 is used in our experiment, and the flours can be treated with transient exposure to non-
90 equilibrium cold plasma. The momentary exposure strategy enhances commercial feasibility,
91 as it can be readily integrated into existing flour processing lines without requiring substantial
92 redesign or major infrastructural modifications, making the approach scalable, energy-
93 efficient, and industry-friendly (24). The transient plasma exposure ensures sufficient
94 interaction between plasma-generated reactive oxygen and nitrogen species (RONS) and flour
95 constituents while minimizing excessive energy input and thermal stress. This short-duration,

96 non-equilibrium treatment helps preserve the intrinsic nutritional and functional attributes of
97 pearl millet flour, while still inducing desirable modifications such as improved hydration
98 behavior, surface activation, and microbial reduction.

99 During the plasma discharge, the presence of electrons, ions, and excited species leads to their
100 interaction with the surrounding air, resulting in the formation of different reactive oxygen-
101 nitrogen species (RONS)(25). The major species believed to be responsible for these reactive
102 oxygen and nitrogen species (RONS) include atomic oxygen (O), ozone (O₃), hydroxyl radicals
103 (OH), nitric oxide (NO), and hydrogen peroxide (H₂O₂) (26,27). Therefore, this study aimed
104 to examine the effects of NECP treatment on several aspects, including nutritional factors,
105 functional and thermal characteristics, changes in pearl millet flour (PMF), and sorghum millet
106 flour (SMF). Furthermore, the effects of NECP treatment on several characteristics of PMF
107 and SMF were examined in further detail using principal component analysis to determine the
108 optimal operating parameters. In addition, the use of NECP treatment might be employed to
109 create functional foods and may have motivated the research community to create more
110 sustainable, environmentally friendly, and energy-efficient technologies for millet processing.
111 By improving flour performance for gluten-free and functional food applications, the work
112 promotes sustainable food diversification and supports resilient food systems. This aligns with
113 UN Sustainable Development Goals (SDG 2: Zero Hunger, SDG 3: Good Health and Well-
114 being, and SDG 12: Responsible Consumption and Production).

115 2. Materials and Methods

116 The pearl millet flour (FMF) and sorghum millet flour (SMF) were obtained from the local
117 market in Jodhpur, Rajasthan, India. The experiments were carried out at ambient temperature
118 in the Cold Plasma Laboratory, located in the Department of Physics at IIT Jodhpur. The
119 analysis was conducted at the Environmental Biotech Lab, located in the Department of
120 Bioscience and Bioengineering at IIT Jodhpur. The functional characteristics, such as Water
121 Holding Capacity (WHC), Oil Holding Capacity (OHC), Water binding capacity (WBC),
122 Dispersibility, color, foaming capacity (FC), and emulsifying capacity (EC), were evaluated
123 for 5- and 10-minute NECP treatment time using the methodologies described elsewhere
124 (20,28). Bioactive compounds like total phenolic content (TPC) and total flavonoid content
125 (TFC) were measured according to Mishra et al. (2024) (29) with slight modification. The
126 Fourier transform infrared spectra of millet flours treated with cold plasma were recorded using
127 FTIR spectroscopy (Bruker, Alpha E FTIR, Germany) with attenuated total reflectance (ATR).



128 The Perkin Elmer DSC-4000, a differential scanning calorimeter, was employed to determine
129 the peak temperatures of finger millet flour treated with plasma.

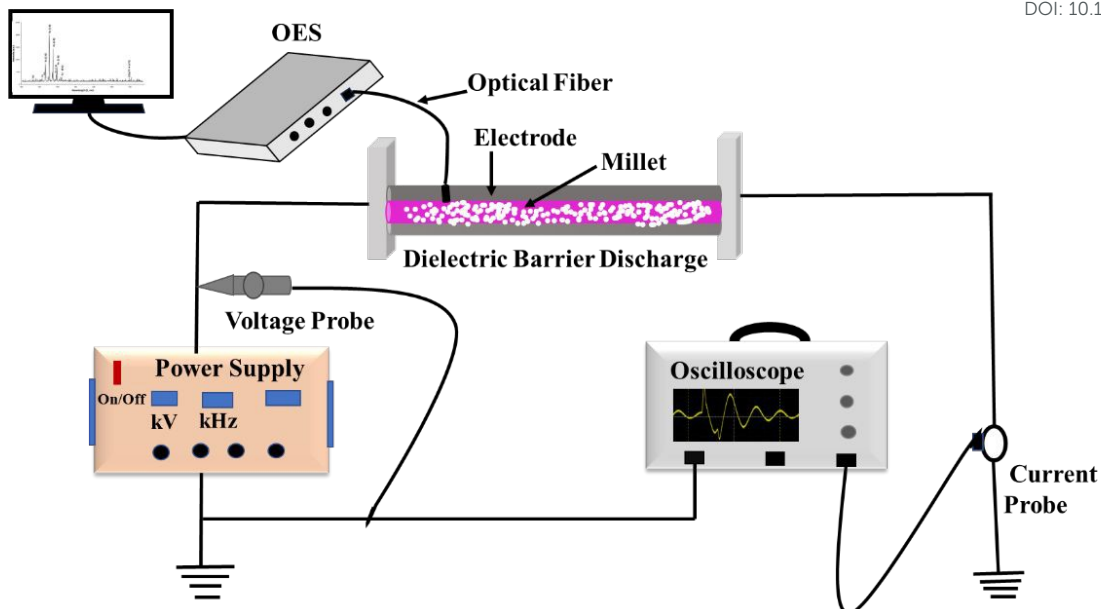
View Article Online
DOI: 10.1039/DSPB00584A

130 **2.1 Experimental setup**

131 The experimental setup implemented for the treatment of the millet flour as shown in Fig. 1
132 The stator and rotator device are powered by the aforementioned variable bipolar pulsed power
133 supply (Grow controls, GC253HVPS), which is coupled with a high voltage probe (1000x,
134 P6015A, Tektronix) and current monitor (Pearson 110) for monitoring the applied voltage (V)
135 and discharge current (I) waveforms which can be directly visualised by a four-channel digital
136 oscilloscope (MDO3014, 100 MHz, Tektronix). The system consists of a Teflon sleeve rotator
137 connected to an aluminium shaft, which is secured to a holder using a nylon gear wheel to
138 maintain a 1.0 mm distance. The stator is composed of an aluminium shaft of the same size,
139 supplied with an identical gear wheel on two side stands. A 1.5 mm thick hollow dielectric
140 material (dielectric constant: 2.1) was placed over a solid aluminium rod measuring 110 mm
141 in length and 15 mm in diameter to cover the stator electrode that was utilized as the cathode.
142 Another aluminium hollow electrode having the same length and diameter as the first, but
143 inside the hollow electrode was used as an anode. The same dielectric material was filled
144 similar to the solid aluminium rod. Plasma discharge was produced at atmospheric pressure,
145 and ambient air was used as the gas carrier between the two electrodes. The high voltage (H.V.)
146 probe was linked to the digital oscilloscope, while a wire connector was used to connect the
147 H.V. probe between the high voltage electrode and the power supply. The high-voltage probe
148 was also appropriately grounded. The wire was attached to the grounded electrode of the device
149 and then passed through a current monitor (CT). The output of the CT was then linked to the
150 digital oscilloscope. The study employed Optical Emission Spectroscopy (OES) (Andor
151 Shamrock SR-500i-B1) to investigate the species produced in an air plasma (Fig. 2). Optical
152 emission spectroscopy (OES) was used to examine the gas phase of cold plasma. The spectrum
153 of dielectric barrier discharge under atmospheric pressure plasma was shown in Fig. 2 from
154 200 to 400 nm and 500 to 900 nm. The spectra from 200 to 400 nm were composed of nitrogen
155 and nitric oxide. NO is produced within the wavelength of 236 to 283 nm. The spectra were
156 characterised by prominent peaks associated with N₂ second positive system (SPS, C-B)
157 emissions at wavelengths of 315.7, 337.3, 353.6, 357.7, 375.5, 380.5 nm (30).

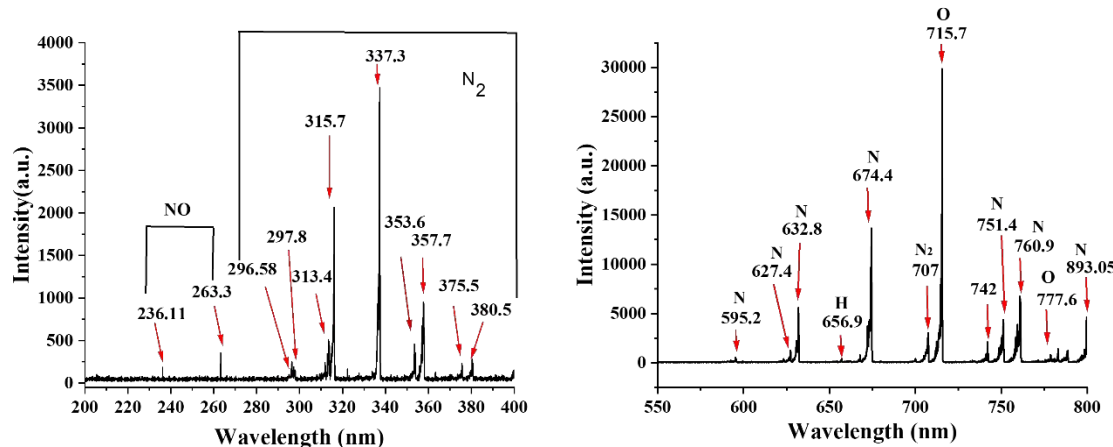
158





159

160 Fig. 1 A schematic illustration of the experimental setup for DBD discharge plasma treatment
161 of millet flour.



162

163 Fig. 2 Optical emission spectrum of DBD Plasma at (a) 200 to 400 nm and (b) 550 to 800 nm

164

165 The preliminary experiments were performed to investigate the treatment efficiency at various
166 voltage levels. It was observed that the plasma discharge initiated at a breakdown voltage of 6
167 kV, stabilized at 7 kV, and remained stable until 9 kV. Due to the impact on the high voltage
168 electrode, it is not suggested to perform prolonged plasma treatments. Moreover, exceeding a
169 specific duration of treatment fails to significantly improve the desired outcomes. Prolonged
170 treatment durations can result in physical harm to the material being treated, including surface
171 erosion, alterations in texture, or compromised structural integrity. Furthermore, when exposed

172 to high voltage for an extended period, the substantial energy released during plasma discharge
173 has the ability to deteriorate nutritional components present in millet flours, including vitamins,
174 amino acids, and antioxidants. Attaining consistent plasma treatment for every individual flour
175 particle can be a challenge. Non-uniform treatment can lead to variations in the quality and
176 functionality of food products. Therefore, we fine-tune our device to achieve the most effective
177 treatment duration. This includes treatment times of up to 20 minutes at 7 KV and up to 10
178 minutes at 9 KV. In our previous work, we used NECP treatment on finger millet flour at 7 KV
179 and found that higher voltage will increase the crystallinity of the flour, thereby increasing its
180 functionality (15). Consequently, the parameters selected for the treatment of PMF and SMF
181 were established as 9 KV for a duration of 5-10 minutes.

182 **2.2 Functional Properties**

183 The functional properties, including Water absorption capacity (WAC), Oil absorption capacity
184 (OAC), Water binding capacity (WBC), Dispersibility, foaming capacity (FC), and
185 emulsifying capacity (EC), were assessed for control as well as NECP-treated pearl millet and
186 sorghum millet flours using the specified methodology (20,28).

187 To obtain water binding capacity (WBC), 1.0 g of millet flour samples was combined with 10
188 ml of deionized water and subjected to centrifugation at 2000 g for 10 min. WBC was
189 calculated using the expression given by Quinton (2002) (31). WBC was determined as the
190 ratio of grams of water retained to grams of solid. The WAC and OAC were determined by
191 employing the methods with minor alterations outlined by Chaple et al. (2020) (28). The WAC
192 and OAC were determined using Equation (1).

193

$$194 \text{WAC and OAC (g/g)} = \frac{\text{Sample weight after centrifugation} - \text{Initial sample weight}}{\text{Initial sample weight}} \quad (1)$$

195

196 **Emulsifying and Foaming Capacity**

197 To determine the emulsifying capacity (EC), a solution containing 0.5 grams of millet flour, 5
198 ml of distilled water, and 5 ml of soybean oil was made in a centrifuge tube. The mixture was
199 mixed using a vortex and then centrifuged at a force of 340 g for 10 minutes. The resulting
200 suspension was carefully transferred to a graduated cylinder, and the total volume as well as
201 the volume of the emulsion layer were precisely measured.

202 The EC (%) was calculated using Equation (2) as specified by Kheto et al. (2022) (32):

203
$$EC\% = \frac{emulsion\ volume\ (mL)}{total\ volume\ (mL)} \times 100 \quad (2)$$

204

205 To measure foaming capacity (FC), 1 gram of millet flour with 50 ml of distilled water was
206 mixed in a beaker. The solution was aggressively stirred for 5 minutes and immediately put
207 into a measuring cylinder. The volume of foam generated was recorded, and FC (%) was
208 determined using Equation (3):

209
$$FC\% = \frac{volume\ after\ shaking\ (mL) - initial\ volume\ of\ suspension}{initial\ volume\ of\ suspension\ (mL)} \times 100 \quad (3)$$

210

211 **Dispersibility**

212 A measured quantity of 10 g of flour was mixed with 100 ml of deionized water, and placed in
213 a 100 ml measuring cylinder. The components are blended and left undisturbed for a duration
214 of 3 hours. The dispersibility of flour was determined by subtracting the volume of settled
215 particles from 100 (33).

216 **2.3 Color**

217 The color values L*, a*, b*, ΔE of PMF and SMF (control and NECP treated) were observed
218 by color reader CR6 (3nh). The L*, a*, b*, ΔE, hue angle, whitening index (WI), yellow index
219 (YI), and browning index (BI) values of PMF and SMF (both control and NECP treated) were
220 determined using equations 4-8 given elsewhere (34,35).

221
$$\text{Hue angle (H)} = \tan^{-1} \frac{b}{a} \quad (4)$$

222
$$\text{Total color difference (ΔE)} = \sqrt{\Delta L^*{}^2 + \Delta a^*{}^2 + \Delta b^*{}^2} \quad (5)$$

223
$$\text{Whitening index (WI)} = \sqrt{(100 - L^*)^2 + a^*{}^2 + b^*{}^2} \quad (6)$$

224
$$\text{Yellow index (YI)} = \frac{142.86b^*}{L^*} \quad (7)$$

225
$$\text{Browning index (BI)} = \frac{[100 \times (X - 0.31)]}{0.172} \quad (8)$$

226 Where, $X = (a^* + 1.75 \times L^*) / (5.645 \times L^* + a^* - 3.012 \times b^*)$

227 **2.4 Bioactive compounds**

228 The sample extracts were prepared according to the procedure outlined by Kheto et al. (2022) Nucle Online
229 (32). Then the prepared sample extract was used to estimate the total phenol content (TPC; g
230 of GAE in 100 g of dm), and total flavonoid content (TFC; g of QE in 100 g of dm).

231 **2.5 Fourier transform infrared spectrometry**

232 The FTIR spectra of the PMF and SMF samples were acquired to assess the functional group
233 variations using a FTIR spectrophotometer (Bruker, Alpha E FTIR, Germany) with attenuated
234 total reflectance (ATR). Samples were gently placed on a ZnSe crystal and scanned at 64 scans
235 per sample to obtain % transmittance at specific wavenumbers ranging from 4000 to 400 cm¹
236 (32)

237 **2.6 Thermal properties**

238 The thermal properties of PMF and SMF samples were determined by a differential scanning
239 calorimeter (Perkin Elmer DSC-4000), to determine the peak temperatures of millet flours
240 treated with plasma in the range of 20 to 220 °C at 10°C per min, as reported by Kheto et al.
241 (2022)(32).

242 **2.7 Field emission Scanning electron microscopy (FESEM) analysis**

243 The morphology of the PMF and SMF samples was examined using a field emission scanning
244 electron microscopy (Thermo Fisher Apreo-2 at 5 kV acceleration voltage). Before imaging,
245 both control and NECP-treated samples were sputtered with gold using a DC sputter. FESEM
246 imaging was then performed to visualize the microstructural variations (24).

247 **2.8 X-ray diffractogram analysis**

248 The PMF and SMF samples were analysed using an X-ray diffractometer (Bruker AXS D8
249 Advance, Germany) to obtain their X-ray diffractograms (XRD). The samples were subjected
250 to an X-ray beam with an intensity of 15 mA and a voltage of 30 kV to investigate the intensity
251 pattern of crystallinity within the 2θ range of 4–45, using a steep angle of 0.02 and a scan rate
252 of 5/min (32).

253 **2.9 Antinutritional factors**

254 To evaluate the influence of NECP on antinutritional components in PMF and SMF, both
255 tannins and phytic acid were quantified in untreated and plasma-treated samples. Tannin
256 analysis was carried out following the procedure described by Yadav et al. (2021)(36). Briefly,
257 1 g of flour was extracted using 10 mL of acidified methanol (HCl: methanol = 1:100), and

258 centrifuged at 6000 rpm for 20 minutes. Then, 1mL of extract was mixed with 5 mL of vanillin
 259 reagent and allowed to react for 20 minutes. The absorbance of the developed color was then
 260 recorded at 500 nm using a UV-visible spectrophotometer (UV-1800, Shimadzu, Japan).
 261 Phytic acid was estimated by the method given by Yadav et al. (2021)(36). Briefly, 0.1 g of the
 262 sample was extracted using 10 mL of 0.2 mol/L hydrochloric acid and allowed to stand for 1
 263 hour. The mixture was then centrifuged at 5000 rpm for 15 minutes, and later 0.5 mL of the
 264 clear supernatant was carefully transferred into a glass-stoppered test tube. An iron (III) reagent
 265 was prepared by dissolving 0.2 g of ammonium iron (III) sulfate dodecahydrate in 100 mL of
 266 2 mol/L HCl and diluting to 1 L with distilled water. Accordingly, 1 mL of this reagent was
 267 added to the sample and the sample was heated for 30 minutes and subsequently cooled in an
 268 ice water bath to 25 °C. Then 2 mL of bipyridine solution (10 g of 2,2'-bipyridine and 10 mL
 269 thioglycolic acid in 1 L of distilled water) was added to the test tube. After 1 minute, absorbance
 270 was recorded at 519 nm using a UV-Vis spectrophotometer (UV-1800, Shimadzu, Japan).

271 **2.10 Statistical analysis**

272 The studies were conducted in triplicate, and the results were provided as the mean standard
 273 deviation. The statistical significance was assessed using the Duncan test. In addition, principal
 274 component analysis (PCA) was conducted using Origin pro 2023 software from OriginLab,
 275 USA, to determine the optimal condition.

276 **3. Results and Discussion**

277 **3.1. Plasma characteristics**

278 A typical V-I characteristic of the above-described DBD source is shown in Fig. 3. The electric
 279 power dissipated into the plasma is calculated from waveforms of applied voltage (U_t) and the
 280 discharge current (i_t), using the following relationship (37) .

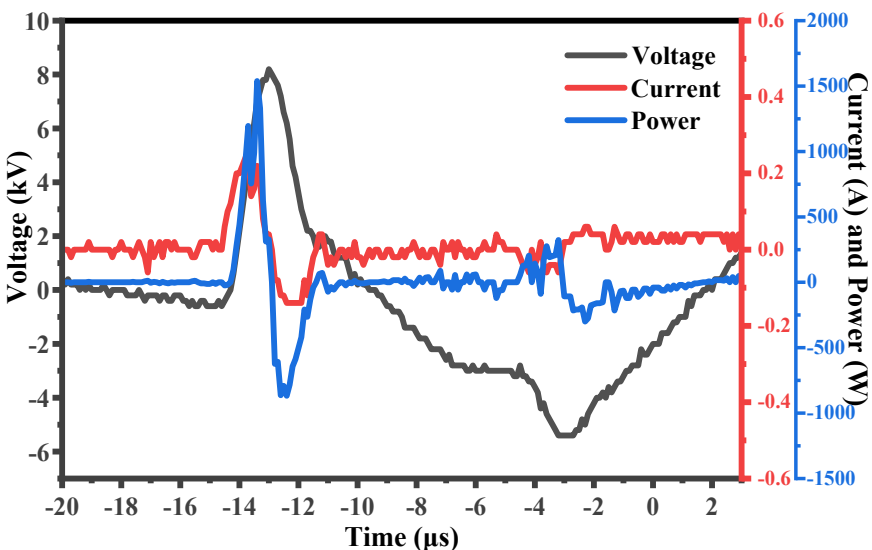
$$281 P_{avg} = \frac{1}{T} \int_0^T P_t dt$$

282 Where T is the period of oscillation, $P(t)$ is the instantaneous power calculated by
 283 multiplying the instantaneous voltage $V(t)$ and current $I(t)$.

284 The electron density can be approximated from the V-I curve using the following
 285 relationship (11):

$$286 n_e = \frac{J}{e\mu_e E} = \frac{I_{rms}}{Ae\mu_e E}$$

287 where J is the current density, A is the cross-sectional area of the powered electrode, I_{rms} is the root mean square current, E is the electric field between the electrodes, e is the electronic charge, and μ_e is the electron mobility, i.e., $552 \text{ cm}^2/\text{V.s}$ in the case of nitrogen. The operational condition results in approximately an average power consumption of 10 W and an electron density of $4.19 \times 10^9 \text{ particles/cm}^3$



292
293 Fig. 3 Typical V–I characteristics for DBD 9 kV/20 kHz.

294 **3.2 Effect of NECP on functional characteristics of millet flour**

295 The functional characteristics of PMF and SMF for control (PMFC and SMFC) and NECP-
296 treated samples for 5 minutes (PMF5 and SMF5) and 10 minutes (PMF10 and SMF10) are
297 presented in Table 1. The functional characteristics of all treated samples were substantially
298 enhanced through NECP-treatment, which was maximum for the 10-minute treated samples.
299 The oil and water absorption capacity of plasma-treated PMF and SMF showed a positive
300 correlation with increasing treatment time. The untreated PMF and SMF exhibited an oil
301 absorption capacity of $1.21 \pm 0.041 \text{ g/g}$ and $1.08 \pm 0.02 \text{ g/g}$, and a water absorption capacity of
302 $1.55 \pm 0.083 \text{ g/g}$ and $1.43 \pm 0.042 \text{ g/g}$, respectively. The OAC of PMF10 and SMF10 had a
303 maximum value of $1.4 \pm 0.034 \text{ g/g}$ and $1.27 \pm 0.015 \text{ g/g}$, which were significantly ($P < 0.05$) higher
304 than the untreated samples (PMFC and SMFC). Similarly, the WAC of PMF10 and SMF10
305 had significantly ($P < 0.05$) higher values, 1.81 ± 0.094 and 1.74 ± 0.08 , compared to the untreated
306 samples. The increase in OAC and WAC is attributed to the existence of plasma-generated
307 species, such as ions and radicals. These species improve the hydrophilic characteristics of
308 flour, with the degree of starch molecule degradation after NECP treatment contributing to this
309 enhancement (38). Furthermore, the degradation of starch is mostly attributed to the influence

of high-energy plasma species and the partial oxidation of starch, particularly by ozone resulting in the formation of carboxylic starch. In addition, it is possible that the sample treated with NECP had a higher concentration of hydrophilic sites, including proteins, carbohydrates, and certain residues of polar amino acids. The NECP treatment causes the depolymerization of starch particles, increasing amylose content. This increase in amylose content leads to an increase in crystallinity, which is also associated with increased water absorption capacity. The FTIR results support these findings. Additionally, the NECP treatment causes the formation of fissures and dents, which provide more sites for lyophilic groups. This ultimately leads to an increase in the oil absorption capacity (OAC) of the flour. Similar findings were reported elsewhere (20,39). However, Chaple et al. (2020) (28) noticed that there were no notable changes in the OAC of wheat flour when exposed to 80kV plasma for durations ranging from 5 to 30 minutes. They observed that the quantities of protein and nonpolar amino acids exhibited fluctuations, although these variations were deemed insignificant. Increased WAC and OAC levels have the intriguing impact of enhancing the volume and texture of baked food products, this attribute makes them well-suited for various baking purposes (40).

The water binding capacity (WBC) of NECP-treated flour was enhanced by the plasma treatment, as shown in Table 1. The WBC of the control (PMFC and SMFC) samples were 2.25 ± 0.059 and 2.01 ± 0.007 , respectively, which had a significantly higher ($P < 0.05$) value for the 10-minute treated samples. The WBC of PMF10 and SMF10 were determined as 2.37 ± 0.021 and 2.26 ± 0.055 , while for PMF5 and SMF5, the value of WBC was recorded as 2.34 ± 0.016 and 2.11 ± 0.003 , respectively. Similarly, Chaple et al. (2020) (28) reported that plasma treatment resulted in an enhancement in the water binding capacity (WBC) of flour. The flour's hydration characteristics are enhanced by plasma treatment, indicating that the higher surface area resulting from the initial plasma treatment influences the hydration qualities of the flours. This information can be considered in order to meet specific functional needs. Furthermore, as compared to the control, the NECP-treated samples showed significantly higher ($P < 0.05$) values for EC and FC. The control PMF and SMF exhibit an EC value of $61.86 \pm 0.51\%$ and $61.29 \pm 0.023\%$ (Table 1), respectively. Following a 10-minute plasma treatment, the EC value exhibited a rise to $64.12 \pm 0.635\%$ and $63.21 \pm 0.084\%$. The increase can be ascribed to the improved disorganized arrangement, which allows the proteins to engage with both water and oil. Consequently, the ability of the emulsion to hold and disperse substances is enhanced, and the creation of air bubbles is increased (41). The FC value of the



342 treated PMF10 and SMF10 significantly increased ($p<0.05$) to $13.18\pm0.282\%$ and [View Article Online](#)
DOI: 10.1039/DSTB00584A
343 $12.19\pm0.337\%$ respectively, compared to the control PMFC and SMFC with an FC value of
344 $11.57\pm0.492\%$ and $10.44\pm0.22\%$, respectively. Sarkar et al. (2023) (21) observed that the
345 plasma treatment of the pearl millet surface leads to the exposure of hydrophobic groups, which
346 in turn attract oil droplets and enhance the stability of the emulsions formed. In addition, the
347 plasma treatment may have raised the surface elasticity; this higher elasticity allows the protein
348 to stretch and deform around the oil droplets and air bubbles, resulting in an enhanced FC (42).
349 The NECP treatment did not affect the dispersibility of the PMF and SMF samples. Similar
350 findings were reported elsewhere (12).

351 **3.3 Bioactive compounds (total phenol content and total flavonoid content)**

352 The NECP treatment did not have a significant impact on the values of total phenolic content
353 and total flavonoid content (TPC) and (TFC), as shown in Table 1. The TPC of the PMFC was
354 determined to be 2.39 ± 0.08 (mg GAE/100 g dm). The TPC decreased as the treatment duration
355 increased from 5 to 10 minutes. The TFC of the PMFC sample was 2.17 ± 0.092 (mg QE/100 g
356 dm), which decreased with the NECP treatment. Similarly, the TFC of SMFC was measured
357 to be 2.22 ± 0.04 , which reduces to 2.14 ± 0.03 and 2.09 ± 0.023 ($p <0.05$) for SMF5 and SMF10,
358 respectively. The TFC has also decreased after NECP treatment, which was recorded as
359 1.65 ± 0.031 for SMF5 and 1.60 ± 0.023 for SMF10, whereas the untreated sample (SMFC) had
360 a TFC value of 1.73 ± 0.05 . The minor decline in TPC (Total Phenolic Content) and TFC (Total
361 Flavonoid Content) indicates that plasma discharge generates high-energy electrons that,
362 through direct interaction with phenolic compounds, induce the dissociation of oxygen
363 molecules and subsequently lead to deterioration (10,12). Furthermore, a decrease in phenolic
364 compounds can potentially contribute to the generation of ozone and other reactive species
365 through dissociation, a process in which individual oxygen atoms unite with oxygen molecules
366 to produce ozone. Conversely, aliphatic molecules, such as hydroxylated and quinone
367 compounds, are produced through the reaction of molecular ozone with the aromatic rings of
368 phenolics, leading to the breakdown and deterioration of phenolic compounds (21). Additional
369 investigation is required to comprehend the interaction between phytochemicals and reactive
370 species. Overall, the recent findings corroborated the results of the previous study by Sarkar et
371 al. (2023) and Almeida et al. (2015) (21,43), which revealed a decrease in phytochemicals
372 following CP treatment.

373

374 Table 1. Effect of NECP on functional characteristics of finger millet flour

		PMFC	PMF5	PMF10	SMFC	SMF5	SMF10
Water Absorption Capacity (WAC) (g/g)		1.55±0.0 83 ^b	1.68±0.0 4 ^{ab}	1.81±0.0 94 ^a	1.43±0.0 4 ^b 2	1.52±0.1 b	1.74±0.0 8 ^a
Oil Absorption Capacity (OAC) (g/g)		1.21± 0.041 ^a	1.28±0.0 3 ^b	1.4±0.03 4 ^c	1.08±0.0 2 ^c	1.15±0.0 3 ^b	1.27±0.0 15 ^a
Water Binding Capacity (WBC) (g/g)		2.25±0.0 59 ^b	2.34±0.0 16 ^a	2.37±0.0 21 ^a	2.01±0.0 07 ^c	2.11±0.0 03 ^b	2.26±0.0 55 ^a
Total Phenol Content (TPC) (mg GAE/100 g dm)		2.39±0.0 8 ^{NS}	2.34±0.0 72 ^{NS}	2.25±0.0 35 ^{NS}	2.22±0.0 4 ^b	2.14±0.0 3 ^{ab}	2.09±0.0 23 ^a
Total Flavonoid Content (TFC) (mg QE/100 g dm)		2.17±0.0 92 ^{NS}	2.16±0.1 1 ^{NS}	2.04±0.0 35 ^{NS}	1.73±0.0 5 ^b	1.65±0.0 31 ^b	1.60±0.0 23 ^a
Emulsifying Capacity (EC) %		61.86±0. 51 ^b	62.38±0. 21 ^b	64.12±0. 635 ^a	61.29±0. 023 ^c	62.33±0. 087 ^b	63.21±0. 084 ^a
Foaming Capacity (FC) %		11.57±0. 492 ^b	12.39±0. 385 ^{ab}	13.18±0. 282 ^a	10.44±0. 22 ^c	11.11±0. 217 ^b	12.19±0. 337 ^a
Dispersibility %		79.02±0. 921 ^b	76.81±0. 737 ^{ab}	74.13±1. 11 ^a	77.78±0. 683 ^c	74.29±0. 858 ^b	71.46±0. 51 ^a

375 Means with different superscripts in the same row represent significant ($p < 0.05$) differences
376 with each other.

377

378 **3.4 Effect of NECP on Color**

379 The color attributes of cold plasma-treated and untreated PMF and SMF were assessed and
380 reported in Table 2. The results were derived using the CIELAB (L^* , a^* , b^*) color space. L^*
381 represents lightness, while a^* and b^* represent red-greenness and blue-yellowness, respectively
382 (44). The L^* value of PMF samples varied between 46.01 ± 0.02 to 46.325 ± 0.175 . The flour
383 experienced no reduction in its L^* value following the NECP treatment. This shows that NECP
384 treatment has no effect on L^* values, indicating similar hue for the treated and untreated PMF
385 samples. The values a^* and b^* of all the samples range from 0.635 ± 0.005 to 0.625 ± 0.035 and

386 from 0.855 ± 0.005 to 0.825 ± 0.015 , respectively. The L^* value of the SMF samples ranged from
 387 47.525 ± 0.015 to 47.395 ± 0.015 . The NECP treatment did not cause any decrease in the L^* value
 388 of the flour. The results demonstrate that NECP treatment does not impact the L^* values,
 389 indicating that the hue of the treated and untreated SMF samples is similar. The values of a^*
 390 and b^* for all the samples vary between 0.855 ± 0.005 and 0.88 ± 0.01 , and between 1.685 ± 0.045
 391 and 1.495 ± 0.015 , respectively. The lack of significant shifts in color values implies that non-
 392 equilibrium cold plasma does not induce any changes in the product's color. The whitening
 393 index (WI), yellow index (YI), and hue angle (h^*) of the plasma-treated pearl millet flour
 394 remains unchanged with the different treatment times. However, there was only a minor overall
 395 change in color observed, and this shift can be attributed to the surface structure of the particles,
 396 which is significantly affected by plasma and is evident in the optical characteristics of flour.
 397 Due to the surface etching caused by plasma treatment, it is expected that there would be
 398 changes in the color values of the treated product (13).

399 Table 2. Effect of NECP on Color of pearl and sorghum millet flour

Color Index	PMFC	PMF5	PMF10	SMFC	SMF5	SMF10
L*	46.01 ± 0.02^N S	46.035 ± 0.015 NS	46.325 ± 0.175 NS	47.525 ± 0.015 a	47.30 ± 0.01^b 5 ^b	47.395 ± 0.01
a*	0.635 ± 0.005 NS	0.655 ± 0.01^N ^S	0.625 ± 0.035^N ^S	0.855 ± 0.005^b	0.82 ± 0.01^b	0.88 ± 0.01^a
b*	0.855 ± 0.005 a	0.825 ± 0.015^b	0.835 ± 0.035^b	1.685 ± 0.045^a	1.475 ± 0.005 b	1.495 ± 0.015^b
hue angle (h*)	1.574 ± 0.012 NS	1.818 ± 0.033^N ^S	1.605 ± 0.089^N ^S	1.227 ± 0.0075 a	1.229 ± 0.01^b	1.136 ± 0.012^c
Whitenin g index (WI)	45.99 ± 0.02 NS	46.02 ± 0.015^N ^S	46.314 ± 0.174 NS	47.491 ± 0.016 a	47.282 ± 0.01 b	47.366 ± 0.01 4 ^b
Yellow Index (YI)	2.654 ± 0.016 a	2.56 ± 0.047^b	2.574 ± 0.098^b	5.065 ± 0.136^a	4.453 ± 0.015 b	4.512 ± 0.043^b

Browning Index	2.826 \pm 0.019	2.627 \pm 0.048 ^b	2.748 \pm 0.048 ^b	4.763 \pm 0.089 ^a	4.343 \pm 0.01 ^b	4.469 \pm 0.015 ^b
Color change	0.11 \pm 0.01 ^c	0.17 \pm 0.01 ^b	0.29 \pm 0.014 ^a	2.525 \pm 0.05 ^a	2.255 \pm 0.015	2.335 \pm 0.025 ^b
ΔE						^b

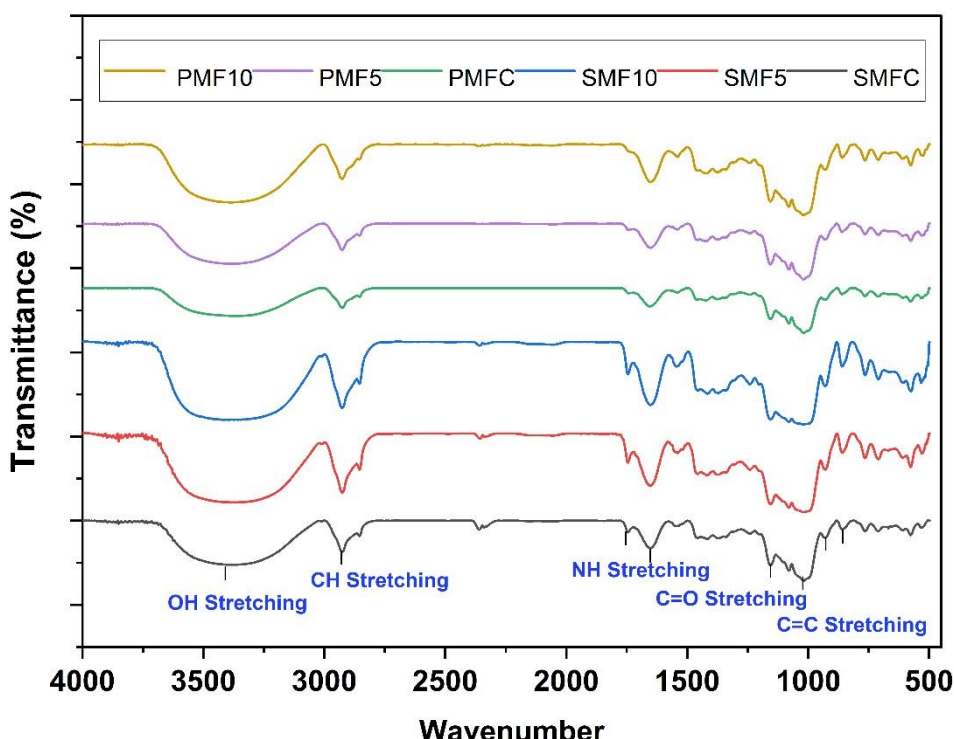
400 Means with different superscripts in the same row represent significant ($p < 0.05$) differences
 401 from each other.

402 **3.5 Fourier transmission infrared spectrum of millet flour**

403 The FTIR spectra of control and NECP-treated PMF and SMF samples are shown in Fig. 4.
 404 The FTIR spectra depicted the C-H stretching vibration, the starch functional groups (O-H),
 405 and the glucose pyranose vibrational twisting patterns in specific locations, namely 2800-3000
 406 cm^{-1} , 3000-3600 cm^{-1} , and 800-1200 cm^{-1} . The range of 1600–1700 cm^{-1} is used to indicate the
 407 stretching of the C O bond, while the range of 1500–1600 cm^{-1} is used to indicate the vibration
 408 of the N H bond. The difference in absorbance observed between the PMF and SMF samples
 409 could indicate a change in functional group concentration due to complexity in their structure.
 410 All treated and control samples had a similar absorbance pattern, indicating that no new
 411 functional groups had formed in the sample; however, there was a difference in the intensity
 412 of NECP-treated samples due to the interaction with free radicals generated during the course
 413 of cold plasma(14). The FTIR spectra of PMF and SMF subjected to treatments of 5 and 10
 414 minutes displayed clearly identifiable peaks, as depicted in the Figure. The sample exhibited a
 415 prominent peak at a wavenumber of 3391 cm^{-1} . This peak elongated in the treated samples,
 416 which is associated with the elongation of OH bonds. The glycosidic bonds of the starch
 417 molecules are being attacked by reactive oxygen and nitrogen species (RONS), which provide
 418 powerful intermolecular interactions via RONS found in the cold plasma (45). The breakdown
 419 of starch components is caused by these bonds, which demonstrate C-H stretching at 2926 and
 420 2849 cm^{-1} . The analysis revealed further peaks at 1746, 1547, 1650, 1162, and 1012 cm^{-1} ,
 421 corresponding to the primary amide, secondary amide of C–O stretching, C–C stretching, and
 422 alkene group of C–C bending, respectively. Zhou et al. (2018) (46) reported the presence of
 423 absorption peaks at 1167 cm^{-1} , 1079 cm^{-1} , and 994 cm^{-1} . Similarly, Chaple et al. (2020)
 424 (28) found analogous peaks in the region of 1600–1700 cm^{-1} . These data suggest that the
 425 starch granules underwent oxidation as a result of the influence of plasma species (10,12). In

426 addition, the transmittance in the 800–1200 cm⁻¹ band for the sample shows an increase
 427 compared to the control, indicating alterations in the crystallinity of starch granules and the
 428 promotion of more organized C–O–C arrangements. The carbonyl groups (C=O) are produced
 429 through the oxidation of hydroxyl (OH) groups in starch by reactive oxygen species (ROS)
 430 created during cold plasma treatment (23).

431



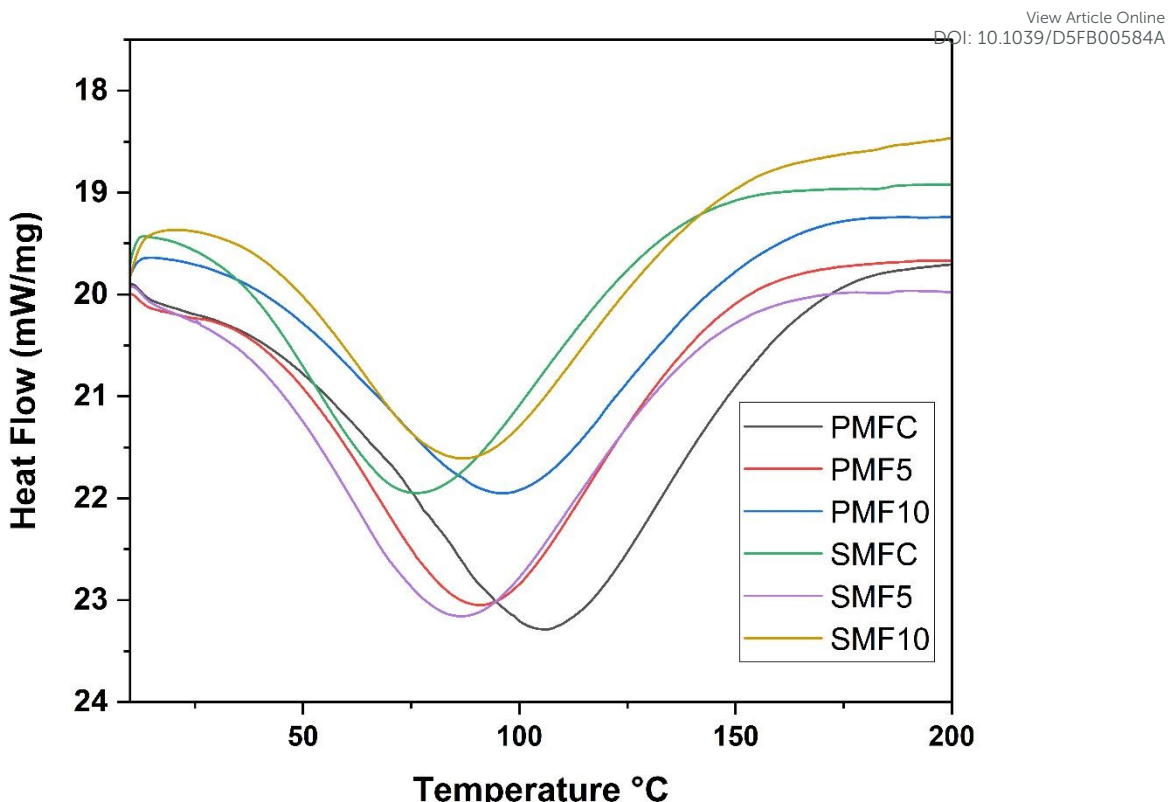
432
 433 Fig. 4 FTIR spectra of PMF and SMF treated with NECP
 434

435 3.6 Thermographs of millet flour

436 Table 3 summarizes the thermal properties of both the control and NECP-treated samples,
 437 which include the onset temperature (To), peak temperature (Tp), and conclusion temperature
 438 (Tc). Thermographs of treated and control PMF and SMF are shown in Fig. 5. The changes in
 439 the physical state and crystalline structure of flour can be caused by either absorbing heat
 440 (endothermic) or releasing heat (exothermic). The gelatinization temperatures of samples
 441 treated with PMF and SMF were somewhat lower in comparison to the untreated samples. The
 442 NECP-treated samples exhibited an earlier onset temperature (To) compared to the untreated
 443 ones. This can be due to a higher level of damage caused by plasma species to the molecular

444 structure of starch. The peak temperature (Tp) of the PMFC was 101.8 °C. In the PMF5 sample
445 the peak temperature decreased to 98.85 °C, while in the PMF10 sample, it decreased further
446 to 93.53 °C. Similarly, the peak temperature (Tp) of the SMF5 and SMF10 decreased to 86.53
447 and 76.37 °C, respectively, compared to the SMFC, which had a temperature of 87.79 °C.
448 Thirumdas et al. (2017) (47) reported a comparable reduction in the gelatinization temperature
449 of rice starch following cold plasma treatment. This endothermic shift is associated with the
450 depolymerization or alteration in the ratio of amylose and amylopectin in starch granules and
451 complete degradation of the starch crystalline structure by NECP-generated species (48).
452 Similarly, the peak temperatures were decreased for little millet flour treated with multipin cold
453 plasma employing varying power and treatment time (20). However, Sarkar et al. (2023) (49)
454 reported that the pearl millet flour samples subjected to cold plasma exhibited a slightly
455 elevated peak temperature (Tp), which could be attributed to the formation of cross-links
456 induced by plasma species. Wongsagonsup et al. (2014) (50) previously documented that the
457 lower plasma power levels cause the plasma species to start the process of connecting starch
458 chains, whereas greater plasma power levels result in the breakdown of starch chains. In our
459 earlier research, we observed that the peak gelatinization temperature increases while using
460 low-power plasma. Therefore, in this investigation, we treated all the samples by applying a
461 higher voltage of approximately 9 kV. The gelatinization enthalpy (ΔH) decreases slightly from
462 194.93 J/g to 153.85 J/g in PMF5 and 150.72 J/g in PMF10. Similarly, gelatinization enthalpy
463 (ΔH) is reduced to 151.53 J/g and 140.37 J/g in SMF5 and SMF10, as compared to untreated
464 SMF, which had a gelatinization enthalpy of 182.76 J/g. The PMF 10 and SMF10 resulted in
465 a significant reduction in the gelatinization enthalpy, with a maximum decrease of 22.67% and
466 23.17% respectively. The reduction in enthalpy indicates that the millet flour treated with non-
467 equilibrium cold plasma requires less energy for gelatinization.





468
469 Fig. 5 Thermograph of untreated and NECP-treated PMF and SMF
470

3.7. Effect of NECP on structural properties of millet flour

471 The Fig.6 illustrates the XRD spectrum used to examine the effect of NECP treatment on the
472 crystal structure of PMF and SMF. The spectra clearly demonstrate the presence of
473 semicrystalline areas in both the PMF and SMF, characterized by a closely packed and
474 organized arrangement of starch molecules. The X-ray diffraction (XRD) patterns of the millet
475 flour samples exhibited wide peaks, suggesting the presence of a type-A crystalline pattern,
476 which is evident from the prominent peaks at 2θ values of 15.14° , 17.12° , 17.94° , 20.04° ,
477 22.94° , and 26.52° . Furthermore, there are dispersed peaks that signify the existence of non-
478 crystalline areas. The crystallinity percentage in PMF increases with NECP treatment, which
479 was 26.48% in PMFC and increased to 29.34% and 31.4% in PMF5 and PMF10, respectively
480 (Table 3). Similarly, the level of crystallinity in the SMF5 (27.18%) and SMF10 (28.63%) was
481 higher than that of the SMFC (25.38%). The increase in crystallinity is attributed to the
482 deterioration of non-crystalline portions of starch molecules caused by NECP treatments. The
483 NECP treatment may have caused alterations in starch granules, such as breakdown and



484 depolymerization, due to interactions with RONS. Moreover, reactive plasma species clash
 485 with starch constituents such as amylose and amylopectin, resulting in an increase in the
 486 number of sites accessible for starch-water interaction and, consequently, an increase in the
 487 water solubility index (51). Kaur & Annapure (2024) (52) reported that the impact of
 488 atmospheric cold plasma on finger millet resulted in an increase in relative crystallinity and
 489 subsequently led to an increase in the water solubility index. Therefore, NECP-treated samples
 490 led to the creation of starches that exhibited greater stability and solubility in comparison to
 491 the control.

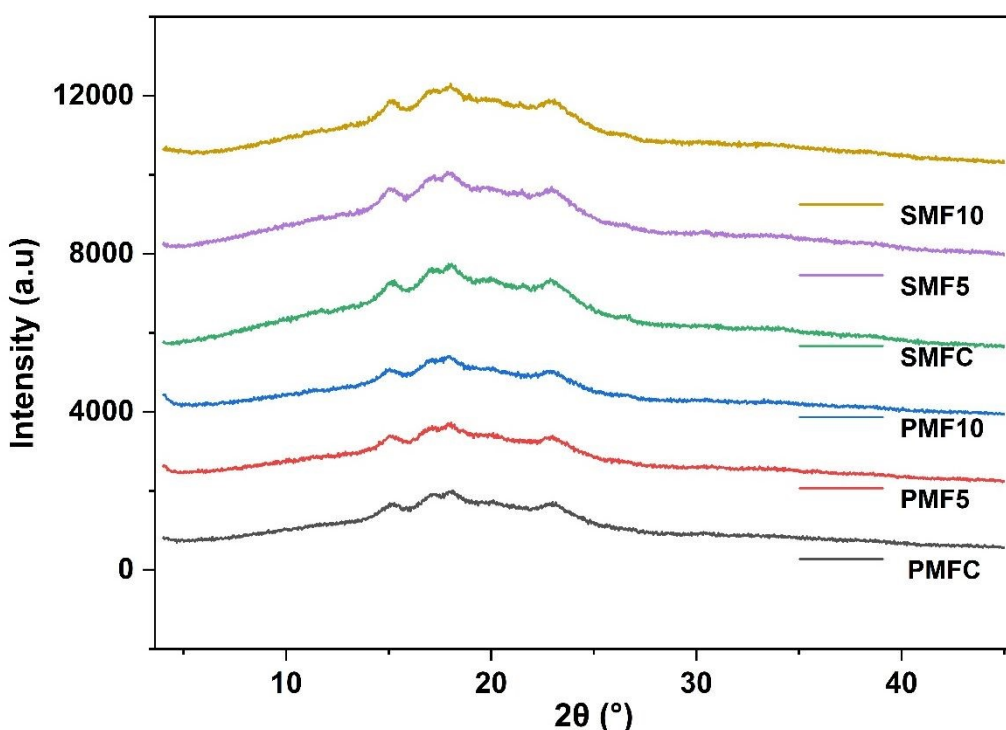
492 Table 3. Effect of NECP on Thermal properties and crystallinity of pearl millet and sorghum
 493 millet flour

494

	To	T _p	T _c	ΔH	Degree of gelatinization	% Crystallinity
	°C	°C	°C	J/g	%	%
PMFC	32.23	101.8	175.25	194.93	NA	26.48
PMF5	31.23	98.85	168.25	153.85	21.07%	29.34
PMF10	29.56	93.53	166.92	150.72	22.07%	31.4
SMFC	38.56	87.79	150.07	182.76	NA	25.38
SMF5	36.73	86.53	157.06	151.53	17.08%	27.187
SMF10	34.4	76.37	162.23	140.37	23.15%	28.635

495





496

497 Fig. 6 Diffractograms of untreated and NECP-treated PMF and SMF

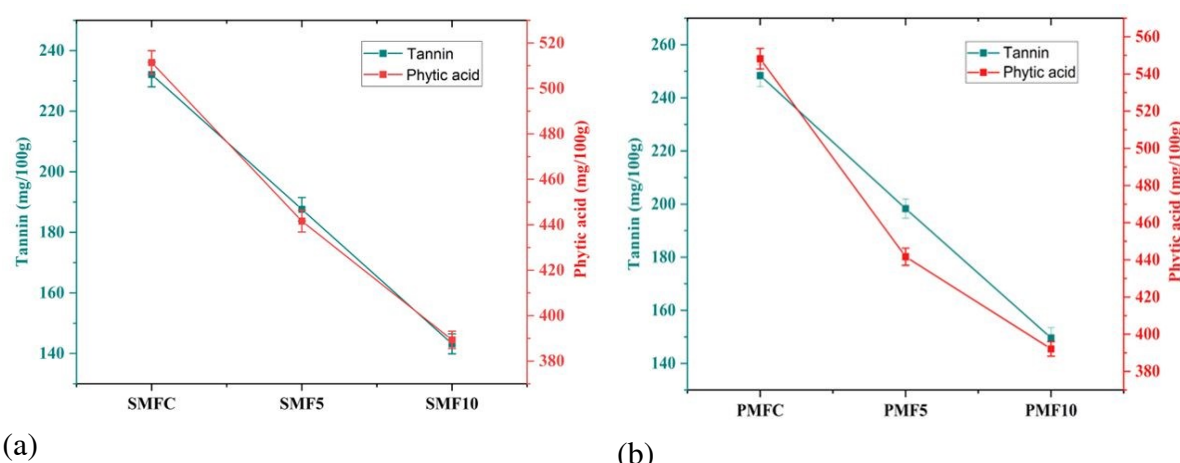
498 **3.8 Effect of NECP on antinutritional factors**

499 The effect of NECP treatment on antinutritional factors in PMF and SMF is illustrated in Fig.
500 7, showing a progressive and significant reduction in both tannin and phytic acid content with
501 increasing treatment time (0, 5, and 10 minutes). In PMF, the tannin content decreased from
502 approximately 250 mg/100 g to 145 mg/100 g, and phytic acid content reduced from 545
503 mg/100 g to 395 mg/100 g. Similarly, in SMF, tannin content declined from 232 mg/100 g to
504 143 mg/100 g, while phytic acid content decreased from 511 mg/100 g to 368 mg/100 g. These
505 results indicate a dose-dependent degradation of antinutritional compounds, attributed to the
506 action of plasma-generated RONS such as hydroxyl radicals ($\bullet\text{OH}$), ozone (O_3), nitric oxide
507 (NO), and peroxynitrite (ONOO^-), which are known to induce oxidative cleavage of phenolic
508 and phosphate-rich compounds (53). Similar observations were reported by Kheto et al. (2023)
509 (41), where atmospheric pressure cold plasma treatment significantly reduced phytic acid and
510 improved protein digestibility in guar seed flour. Likewise, R L et al. (2021) (16) demonstrated
511 that cold plasma exposure decreased phytic acid content in pearl millet by up to 60.66%,
512 attributing the effect to oxidative breakdown of phytate rings and possible activation of
513 endogenous phytase enzymes. In another study, Pankaj et al. (2018) (54) emphasized the ability
514 of plasma to disrupt antinutritional factors in legumes and cereals without compromising the



515 structural integrity of starch and protein fractions. The parallel downward trends of tannins and
 516 phytic acid in the current study suggest that both compounds are similarly susceptible to
 517 oxidative degradation, supporting the hypothesis that cold plasma can act as a non-thermal,
 518 residue-free processing tool for improving the nutritional and functional properties of millet
 519 flours. The minimal variability observed in replicates (indicated by small error bars) confirms
 520 the reproducibility and consistency of the treatment. These findings validate NECP as a
 521 sustainable and scalable intervention for enhancing millet flour quality, especially for
 522 applications in functional food formulations where digestibility and mineral bioavailability are
 523 critical.

524



525 Fig. 7 Tannin and phytic acid in untreated and NECP-treated (a) SMF and (b) PMF

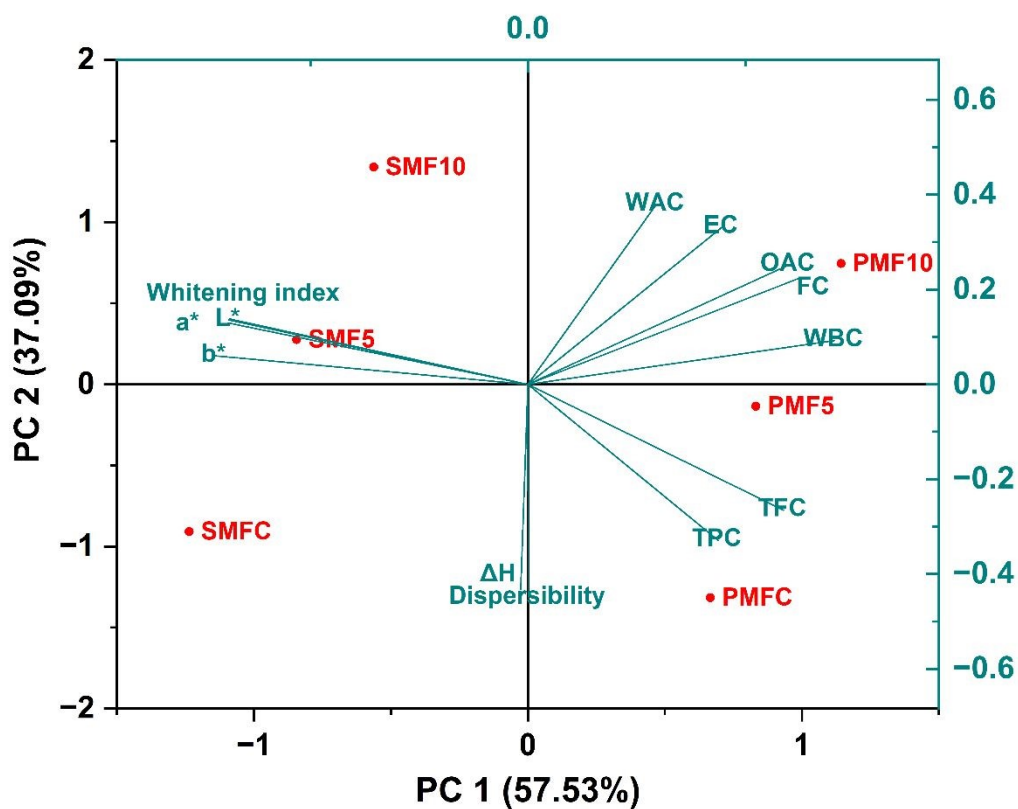
526

527 3.9 Principal component analysis

528 The study examined the correlations between the functional, bioactive chemicals, color, and
 529 thermal properties using Principal Component Analysis (PCA). The results revealed two
 530 principal components, PC1 (57.33%) and PC2 (37.09%), which accounted for a total of 94.42%
 531 of the overall variation (Fig. 8). None of the variables are directly related to any PCs. The
 532 untreated samples of SMFC and PMFC were located in the lower left and right quadrants,
 533 respectively, indicating disparities in the characteristics of the SMF and PMF samples. While
 534 NECP treated SMF10, SMF5, and PMF10, the samples were positioned in the upper left and
 535 right quadrants, which suggests notable variations in characteristics compared to the untreated
 536 samples. This suggests that a prolonged period of plasma treatment, specifically 10 minutes, is

537 required for the plasma-generated reactive oxygen and nitrogen species (RONS) to sufficiently
 538 engage with the flour and influence the functionality of the treated samples.

539 While these results highlight the promise of NECP as an emerging alternative to conventional
 540 thermal processing, still there are certain challenges. The generation and distribution of reactive
 541 species can fluctuate depending on humidity, gas composition, and processing distance and
 542 may affect reproducibility. Potential oxidative changes to lipids or sensitive bioactive
 543 components may also occur under prolonged exposure, which raises questions regarding long-
 544 term storage stability. Lack of established treatment protocols, limited continuous-processing
 545 designs, and the requirement for energy-efficiency evaluation are additional obstacles to
 546 industrial-scale implementation. Therefore, although NECP demonstrates strong potential for
 547 quality enhancement of millet flours, further research is required to address these constraints,
 548 particularly by investigating long-term shelf stability, optimizing process uniformity, and
 549 validating its technological applicability across diverse food matrices. In addition, further study
 550 is required to confirm the suitability of the NECP treatment to improve the functionality of the
 551 millet flour.



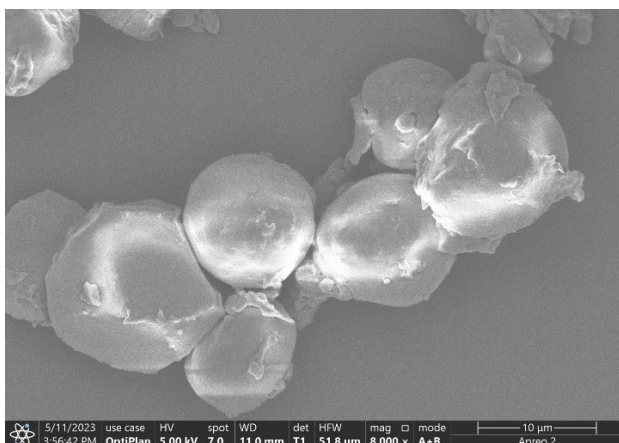
552
 553 Fig. 8 Biplot of PCA analysis of NECP-treated pearl sorghum millet flour.
 554 **3.10 Effect on Microstructural Changes**

555 The microstructural changes induced by NECP treatment in PMF and SMF were examined
556 using FESEM and are shown in Fig. 9. The control samples exhibited compact, well-defined
557 starch granules with smooth, intact surfaces, reflecting minimal structural disturbance. In
558 contrast, the NECP-treated samples showed noticeable morphological alterations, with the
559 degree of surface disruption increasing progressively with treatment duration. For the 5-minute
560 NECP treatment (PMF5 and SMF5), the granules began to show subtle surface roughening,
561 shallow pits, and minor fissures. These features suggest the initial stages of etching is caused
562 by plasma-generated reactive species. The interaction of ions, radicals, and excited molecules
563 with the granule surface likely resulted in partial removal of the outer layers and weakening of
564 amorphous regions. The effect was more pronounced in the 10-minute treated samples (PMF10
565 and SMF10), where the granules displayed significant erosion, deeper cracks, and hollowed
566 regions. Such extensive disruption indicates increased penetration of plasma ions into the
567 granular matrix, leading to degradation of amorphous domains and destabilization of the
568 surface architecture. The stronger etching at longer exposure times is consistent with intensified
569 interaction of RONS with starch and protein components.

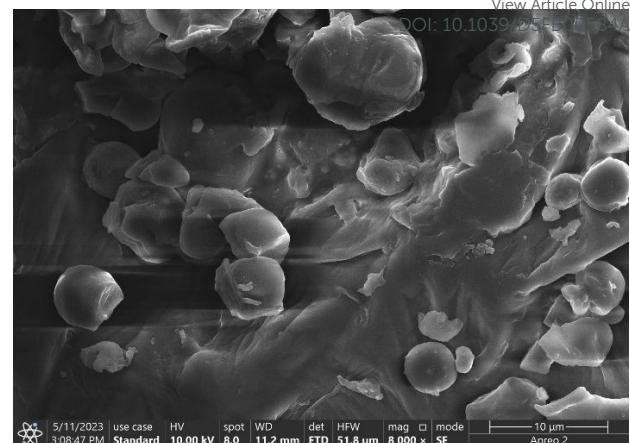
570 The FESEM observations are well supported by the structural and thermal transitions reflected
571 in the XRD and DSC analyses. The progressive surface erosion, fissures, and granular
572 disruption seen in NECP-treated PMF and SMF correspond with the increase in relative
573 crystallinity observed in the XRD patterns. The breakdown of amorphous regions by plasma-
574 generated reactive species likely facilitated the reorganization of remaining starch chains into
575 more ordered crystalline domains, as reflected by the higher crystallinity values in PMF10 and
576 SMF10. This structural rearrangement also aligns with the decrease in gelatinization enthalpy
577 (ΔH) and the shift toward lower onset and peak gelatinization temperatures in the DSC
578 thermograms. These findings are consistent with earlier studies reporting that cold plasma
579 exposure causes surface etching, deformation of granules, and the development of cavities in
580 starch and protein-based systems (55–58). The microstructural breakdown observed in PMF10
581 and SMF10 supports the enhanced functional and thermal properties discussed earlier, as
582 plasma-induced surface roughness and fissures increase the accessibility of hydrophilic and
583 hydrophobic sites, thereby influencing absorption, gelatinization, and solubility behaviour
584 (59).

View Article Online

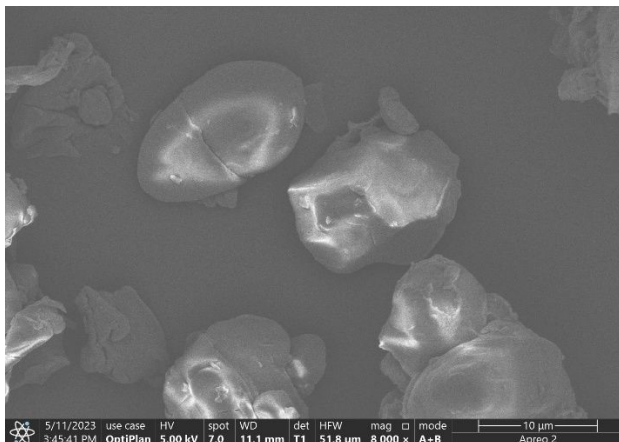
DOI: 10.1039/C5FT00253A



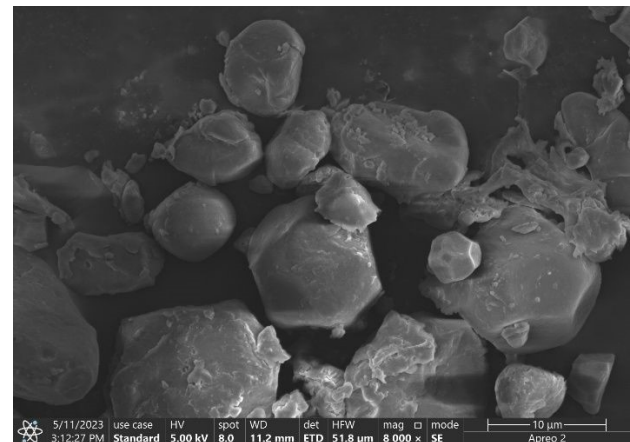
PMF C



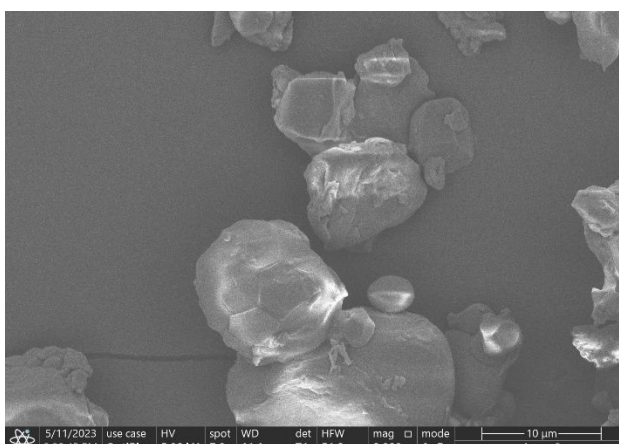
SMF C



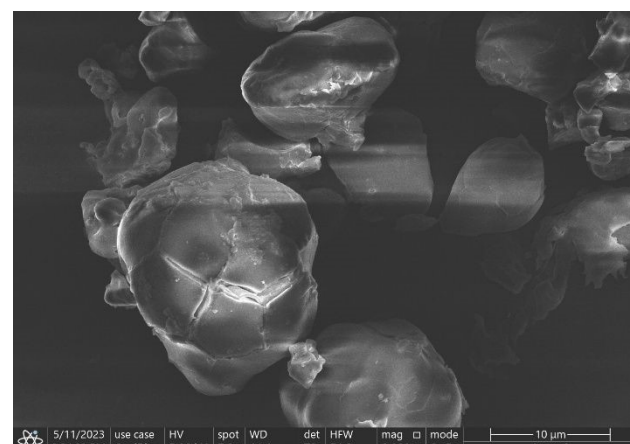
PMF 5



SMF 5



PMF 10



SMF 10

585 Fig. 9 FESEM images of NECP-treated PMF and SMF

587 **4. Conclusions**

588 This study illustrates the efficiency of non-equilibrium cold plasma treatment using a DBD
589 source made of a stator and a rotator electrode arrangement. These features enable easy
590 scalability and enhance commercial viability without requiring significant redesign. The
591 application of NECP treatment to pearl and sorghum millet flour resulted in notable changes
592 to its functional and physical properties. Specifically, the treatment led to a decrease in
593 dispersibility, alongside increases in oil holding capacity, water holding capacity, and water
594 binding capacity. Importantly, no color changes were observed post-treatment. The increase in
595 peak gelatinization temperature is attributed to the depolymerization of starch molecules
596 induced by the plasma treatment. Overall, the enhanced functional properties of pearl and
597 sorghum millet flour post-NECP treatment suggest its potential as a potent component for novel
598 food formulations, such as breads, porridges, and frozen goods. NECP emerges as a promising
599 alternative to traditional heat processing methods, offering a means to improve the quality of
600 millet flour without compromising its physical properties. These findings highlight the
601 potential of NECP to alter the physical and functional characteristics of millet flour, making it
602 a potent component for the food industry.

603 However, further research is necessary to validate the suitability of plasma-treated millet flour
604 for broader applications within the food industry.

605 **Author contributions**

606 Ritesh Mishra - wrote the original draft, contributed to review and editing, and was responsible
607 for visualization, software, methodology, investigation, formal analysis, data curation, and
608 conceptualization. Sushma Jangra - methodology, formal analysis, and investigation. Abhijit
609 Mishra – methodology, investigation, and data curation. Shikha Pandey – methodology and
610 data curation. Meenu Chhabra - review and editing, conceptualization, and supervision. Ram
611 Prakash - review and editing, visualization, conceptualization, and supervision.

612 **Conflicts of interest**

613 The authors declare that they have no conflict of interest.

614 **Data availability**

615 All the data is presented within the manuscript itself.

616 **Acknowledgements**

617 The authors gratefully acknowledge the CRDSI and the AIOT, IIT Jodhpur, for providing the
618 facilities, technical support, and instrumentation required to carry out this research.

619 References

- 620 1. Panwar P, Dubey A, Verma AK. Evaluation of nutraceutical and antinutritional
621 properties in barnyard and finger millet varieties grown in Himalayan region. *J Food
622 Sci Technol.* 2016 Jun 20;53(6):2779–87.
- 623 2. Falguera V, Aliguer N, Falguera M. An integrated approach to current trends in food
624 consumption: Moving toward functional and organic products? *Food Control.* 2012
625 Aug;26(2):274–81.
- 626 3. Conte P. Technological and Nutritional Challenges, and Novelty in Gluten-Free
627 Breadmaking: a Review. *Pol J Food Nutr Sci.* 2019 Mar 1;69(1):5–21.
- 628 4. Joshi TJ, Singh SM, Rao PS. Novel thermal and non-thermal millet processing
629 technologies: advances and research trends. *European Food Research and Technology.*
630 2023 May 7;249(5):1149–60.
- 631 5. Yousaf L, Hou D, Liaqat H, Shen Q. Millet: A review of its nutritional and functional
632 changes during processing. *Food Research International.* 2021 Apr;142:110197.
- 633 6. Mishra R, Chhabra M, Prakash R. Non-equilibrium cold plasmas and their impacts on
634 physico-chemical properties of food items. *Rev Mod Plasma Phys.* 2025 Apr
635 25;9(1):16.
- 636 7. Jangra S, Mishra R, Mishra A, Pandey S, Prakash R. Analysis of short-term treatment
637 effects of dielectric barrier discharge plasma to improve germination characteristics of
638 wheat seeds. *Radiation Effects and Defects in Solids.* 2024 Jul 3;179(7–8):1023–31.
- 639 8. Mishra R, Pandey S, Jangra S, Mishra A, Chhabra M, Prakash R. Effective microbial
640 control, enhancing antioxidant activity and pesticide removal in fresh cut apples with
641 plasma activated water. *Postharvest Biol Technol.* 2025 Oct;228:113660.
- 642 9. Pandey S, Jangra R, Ahlawat K, Mishra R, Mishra A, Jangra S, et al. Selective
643 generation of nitrate and nitrite in plasma activated water and its physicochemical
644 parameters analysis. *Physics Letters, Section A: General, Atomic and Solid State
645 Physics [Internet].* 2023;474:128832. Available from:
646 <https://doi.org/10.1016/j.physleta.2023.128832>
- 647 10. Misra NN, Kaur S, Tiwari BK, Kaur A, Singh N, Cullen PJ. Atmospheric pressure
648 cold plasma (ACP) treatment of wheat flour. *Food Hydrocoll.* 2015 Feb;44:115–21.
- 649 11. Jangra S, Mishra R, Mishra A, Pandey S, Prakash R. Enhancing Physicochemical and
650 Functional Properties of Wheat Flour by Dielectric Barrier Discharge Plasma
651 Treatment. *ACS Food Science & Technology.* 2025 Mar 13;
- 652 12. Jaddu S, Pradhan RC, Dwivedi M. Effect of multipin atmospheric cold plasma
653 discharge on functional properties of little millet (*Panicum miliare*) flour. *Innovative
654 Food Science & Emerging Technologies.* 2022 May;77:102957.
- 655 13. K Joy J, Kalaivandan RGT, Eazhumalai G, Kahar SP, Annapure US. Effect of pin-to-
656 plate atmospheric cold plasma on jackfruit seed flour functionality modification.
657 *Innovative Food Science & Emerging Technologies.* 2022 Jun;78:103009.



658 14. Zare L, Mollakhalili-Meybodi N, Fallahzadeh H, Arab M. Effect of atmospheric [View Article Online](#)
659 pressure cold plasma (ACP) treatment on the technological characteristics of quinoa
660 flour. *LWT*. 2022 Feb;155:112898. DOI:10.1039/D5FB00584A

661 15. Mishra R, Jangra S, Mishra A, Pandey S, Prakash R, Chhabra M. Enhancement of
662 structural and functional characteristics of millet flours using non-equilibrium cold
663 plasma. *Radiation Effects and Defects in Solids*. 2024 Jul 3;179(7–8):881–7.

664 16. R L, P. S S, R M. Improvement in Millet Soaking by Way of Bubbled Cold Plasma
665 Processed Air Exposure; Phytic Acid Reduction Cum Nutrient Analysis Concern.
666 *Frontiers in Advanced Materials Research*. 2021 Oct 30;1–16.

667 17. Sun X, Saleh ASM, Lu Y, Sun Z, Zhang X, Ge X, et al. Effects of ultra-high pressure
668 combined with cold plasma on structural, physicochemical, and digestive properties of
669 proso millet starch. *Int J Biol Macromol*. 2022 Jul;212:146–54.

670 18. Rao M, Akhil K, ... CSIntJC, 2021 undefined. Effect of microwave treatment on
671 physical and functional properties of foxtail millet flour. [researchgate.net](#) [Internet].
672 2021 Jan 1 [cited 2023 May 5];9(1):2762–7. Available from:
673 https://www.researchgate.net/profile/Sunil-C-K/publication/349237467_Effect_of_microwave_treatment_on_physical_and_functional_properties_of_foxtail_millet_flour/links/60261ccb299bf1cc26bce9c8/Effect-of-microwave-treatment-on-physical-and-functional-properties-of-foxtail-millet-flour.pdf

674 19. Jaddu S, Abdullah S, Dwivedi M, Pradhan RC. Multipin cold plasma electric discharge
675 on hydration properties of kodo millet flour: Modelling and optimization using
676 response surface methodology and artificial neural network – Genetic algorithm. *Food
677 Chemistry: Molecular Sciences*. 2022 Dec;5:100132.

678 20. Jaddu S, Pradhan RC, Dwivedi M. Effect of multipin atmospheric cold plasma
679 discharge on functional properties of little millet (*Panicum miliare*) flour. *Innovative
680 Food Science & Emerging Technologies*. 2022 May;77:102957.

681 21. Sarkar A, Niranjan T, Patel G, Kheto A, Tiwari BK, Dwivedi M. Impact of cold
682 plasma treatment on nutritional, antinutritional, functional, thermal, rheological, and
683 structural properties of pearl millet flour. *J Food Process Eng*. 2023 May 15;46(5).

684 22. Sarkar A, Niranjan T, Patel G, Kheto A, Tiwari BK, Dwivedi M. Impact of cold
685 plasma treatment on nutritional, antinutritional, functional, thermal, rheological, and
686 structural properties of pearl millet flour. *J Food Process Eng*. 2023 May 15;46(5).

687 23. Sharma V, Tomar MS, Sahoo S, Pradhan RC. Development of barnyard millet flour
688 rich in bioactive compounds with enhanced functional properties by application of
689 multipin atmospheric cold plasma. *J Food Process Eng*. 2024 Jun 20;47(6).

690 24. Jangra S, Mishra A, Mishra R, Pandey S, Prakash R. Transformative impact of
691 atmospheric cold plasma on mung bean seeds: Unveiling surface characteristics,
692 physicochemical alterations, and enhanced germination potential. *AIP Adv*. 2024 Jul
693 1;14(7).

694 25. Mishra A, Mishra R, Siddiqui YH, Jangra S, Pandey S, Prakash R. Analysis of
695 discharge parameters of an Argon Cold Atmospheric Pressure Plasma Jet and its
696 impact on surface characteristics of White Grapes. *Phys Scr*. 2024 Sep 16;

697 26. Attri P, Ishikawa K, Okumura T, Koga K, Shiratani M. Plasma Agriculture from
698 Laboratory to Farm: A Review. *Processes*. 2020 Aug 17;8(8):1002.



View Article Online
DOI: 10.1039/D5FB00584A

702 27. Pandey S, Mishra R, Mishra A, Jangra S, Prakash R. Plasma Activated Water
703 Generation in Pin-to-Plate Gas Phase DBD-based Plasma Source for Enhanced
704 Biochemical Activity. *Phys Lett A*. 2025 Jan;130245.
705 28. Chaple S, Sarangapani C, Jones J, Carey E, Causeret L, Genson A, et al. Effect of
706 atmospheric cold plasma on the functional properties of whole wheat (*Triticum*
707 *aestivum* L.) grain and wheat flour. *Innovative Food Science & Emerging*
708 *Technologies*. 2020 Dec;66:102529.
709 29. Mishra R, Mishra A, Jangra S, Pandey S, Chhabra M, Prakash R. Process parameters
710 optimization for red globe grapes to enhance shelf-life using non-equilibrium cold
711 plasma jet. *Postharvest Biol Technol*. 2024 Apr;210:112778.
712 30. Mishra A, Jangra S, Mishra R, Pandey S, Soundharajan P, Kombade SP, et al.
713 Characterization Study of a Helium Cold Atmospheric-Pressure Plasma Jet and Its
714 Application in Plasma-Mediated Root Canal Irrigation. *IEEE Trans Radiat Plasma*
715 *Med Sci*. 2025;1–1.
716 31. Quinton L. American Association of Cereal Chemists Approved Methods, 10th ed.,
717 CD-ROM American Association of Cereal Chemists, 2000, ISBN: 1-891127-13-6,
718 US\$579. *Carbohydr Polym*. 2002 Sep 1;49(4):515.
719 32. Khero A, Joseph D, Islam M, Dhua S, Das R, Kumar Y, et al. Microwave roasting
720 induced structural, morphological, antioxidant, and functional attributes of Quinoa (*Chenopodium quinoa* Willd). *J Food Process Preserv*. 2022 May 8;46(5).
721 33. Kulkarni KD, Kulkarni DN, Ingle UM. Sorghum Malt-Based Weaning Food
722 Formulations: Preparation, Functional Properties, and Nutritive Value. *Food Nutr Bull*.
723 1991 Dec 1;13(4):1–7.
724 34. Pathare PB, Opara UL, Al-Said FAJ. Colour Measurement and Analysis in Fresh and
725 Processed Foods: A Review. *Food Bioproc Tech*. 2013 Jan 11;6(1):36–60.
726 35. Ali HM, El-Gizawy AM, El-Bassiouny REI, Saleh MA. The role of various amino
727 acids in enzymatic browning process in potato tubers, and identifying the browning
728 products. *Food Chem*. 2016 Feb;192:879–85.
729 36. Yadav S, Mishra S, Pradhan RC. Ultrasound-assisted hydration of finger millet
730 (*Eleusine Coracana*) and its effects on starch isolates and antinutrients. *Ultrason*
731 *Sonochem*. 2021 May;73:105542.
732 37. Mishra A, P. S, Kumar P, Prakash R. Comparative analysis of disinfection
733 effectiveness of Helium CAP jet, sodium hypochlorite and QMix in *Enterococcus*
734 *faecalis* infected root canals. *Radiation Effects and Defects in Solids*. 2024 Jul
735 3;179(7–8):1009–16.
736 38. Damodaran S, Paraf A. *Food Proteins and their Applications*. CRC Press; 2017.
737 39. Sarangapani C, Thirumdas R, Devi Y, Trimukhe A, Deshmukh RR, Annapure US.
738 Effect of low-pressure plasma on physico-chemical and functional properties of
739 parboiled rice flour. *LWT - Food Science and Technology*. 2016 Jun;69:482–9.
740 40. Iwe MO, Onyeukwu U, Agiriga AN. Proximate, functional and pasting properties of
741 FARO 44 rice, African yam bean and brown cowpea seeds composite flour. *Cogent*
742 *Food Agric*. 2016 Feb 10;2(1).
743 41. Khero A, Mallik A, Sehrawat R, Gul K, Routray W. Atmospheric cold plasma induced
744 nutritional & anti-nutritional, molecular modifications and in-vitro protein



746 digestibility of guar seed (*Cyamopsis tetragonoloba* L.) flour. *Food Research*
747 International. 2023 Jun;168:112790.

748 42. Hoque M, McDonagh C, Tiwari BK, Kerry JP, Pathania S. Effect of Cold Plasma
749 Treatment on the Packaging Properties of Biopolymer-Based Films: A Review.
750 *Applied Sciences*. 2022 Jan 27;12(3):1346.

751 43. Almeida FDL, Cavalcante RS, Cullen PJ, Frias JM, Bourke P, Fernandes FAN, et al.
752 Effects of atmospheric cold plasma and ozone on prebiotic orange juice. *Innovative*
753 *Food Science & Emerging Technologies*. 2015 Dec;32:127–35.

754 44. Mishra R, Mishra A, Jangra S, Pandey S, Chhabra M, Prakash R. Process parameters
755 optimization for red globe grapes to enhance shelf-life using non-equilibrium cold
756 plasma jet. *Postharvest Biol Technol*. 2024 Apr;210:112778.

757 45. Sarkar A, Nirajan T, Patel G, Kheti A, Tiwari BK, Dwivedi M. Impact of cold
758 plasma treatment on nutritional, antinutritional, functional, thermal, rheological, and
759 structural properties of pearl millet flour. *J Food Process Eng*. 2023 May 15;46(5).

760 46. Zhou Y, Yan Y, Shi M, Liu Y. Effect of an Atmospheric Pressure Plasma Jet on the
761 Structure and Physicochemical Properties of Waxy and Normal Maize Starch.
762 *Polymers (Basel)*. 2018 Dec 21;11(1):8.

763 47. Thirumdas R, Trimukhe A, Deshmukh RR, Annapure US. Functional and rheological
764 properties of cold plasma treated rice starch. *Carbohydr Polym*. 2017 Feb;157:1723–
765 31.

766 48. Sumathi A, Ushakumari SR, Malleshi NG. Physico-chemical characteristics,
767 nutritional quality and shelf-life of pearl millet based extrusion cooked supplementary
768 foods. *Int J Food Sci Nutr*. 2007 Jan 6;58(5):350–62.

769 49. Sarkar A, Nirajan T, Patel G, Kheti A, Tiwari BK, Dwivedi M. Impact of cold
770 plasma treatment on nutritional, antinutritional, functional, thermal, rheological, and
771 structural properties of pearl millet flour. *J Food Process Eng*. 2023 May 15;46(5).

772 50. Wongsagonsup R, Deeyai P, Chaiwat W, Horrungsiwat S, Leejariensuk K,
773 Suphantharika M, et al. Modification of tapioca starch by non-chemical route using jet
774 atmospheric argon plasma. *Carbohydr Polym*. 2014 Feb;102:790–8.

775 51. da Costa Pinto C, Sanches EA, Clerici MTPS, Rodrigues S, Fernandes FAN, de Souza
776 SM, et al. Modulation of the Physicochemical Properties of Aria (*Goeppertia allouia*)
777 Starch by Cold Plasma: Effect of Excitation Frequency. *Food Bioproc Tech*. 2023 Apr
778 15;16(4):768–84.

779 52. Kaur P, Annapure US. Understanding the atmospheric cold plasma-induced
780 modification of finger millet (*Eleusine coracana*) starch and its related mechanisms. *Int*
781 *J Biol Macromol*. 2024 May;268:131615.

782 53. Misra NN, Yadav B, Roopesh MS, Jo C. Cold Plasma for Effective Fungal and
783 Mycotoxin Control in Foods: Mechanisms, Inactivation Effects, and Applications.
784 *Compr Rev Food Sci Food Saf*. 2019 Jan 18;18(1):106–20.

785 54. Pankaj SK, Wan Z, Keener KM. Effects of Cold Plasma on Food Quality: A Review.
786 *Foods* 2018, Vol 7, Page 4 [Internet]. 2018 Jan 1 [cited 2021 Aug 21];7(1):4. Available
787 from: <https://www.mdpi.com/2304-8158/7/1/4/htm>

788 55. Jaddu S, Pradhan RC, Dwivedi M. Effect of multipin atmospheric cold plasma
789 discharge on functional properties of little millet (*Panicum miliare*) flour. *Innovative*
790 *Food Science & Emerging Technologies*. 2022 May;77:102957.



791 56. Sarkar A, Niranjan T, Patel G, Kheto A, Tiwari BK, Dwivedi M. Impact of cold plasma treatment on nutritional, antinutritional, functional, thermal, rheological, and structural properties of pearl millet flour. *J Food Process Eng.* 2023 May 15;46(5). [View Article Online](#) DOI:10.1039/D5FB00584A

792 57. Sun X, Saleh ASM, Sun Z, Ge X, Shen H, Zhang Q, et al. Modification of multi-scale structure, physicochemical properties, and digestibility of rice starch via microwave and cold plasma treatments. *LWT.* 2022 Jan;153:112483.

793 58. Gong W, Guo X lu, Huang H bo, Li X, Xu Y, Hu JN. Structural characterization of modified whey protein isolates using cold plasma treatment and its applications in emulsion oleogels. *Food Chem.* 2021 Sep;356:129703.

794 59. K Joy J, Kalaivandan RGT, Eazhumalai G, Kahar SP, Annapure US. Effect of pin-to-plate atmospheric cold plasma on jackfruit seed flour functionality modification. *Innovative Food Science & Emerging Technologies.* 2022 Jun;78:103009.

795

796

797

798

799

800

801

802

803

Data availability

All the data is presented within the manuscript itself.